Theory of star formation

Monday 8th

- 17.15 – 18.00 Molecular clouds and star formation: Introduction

Tuesday 9th

- 13.15 – 14.00 Molecular clouds: structure, physics, and chemistry
- 16.00 – 16.45 Cloud cores: statistics and evolution

Wednesday 10th

- **11.15 – 12.00 Protostars**

Protostars

The goals

- know basic models of low-mass/high-mass star formation
- know the basic constituents of a protostar
- know tracers available for the study of protostellar systems

Protostar

- collapse of a cloud core results in the formation of protostar(s)
  - object whose luminosity results mainly from accretion
  - accretion ongoing, gravitational energy is transformed into heating of the gas
  - pre-main sequence phase = fusion reactions have not yet started
    - hydrogen fusion requires ~10^7 K
    - if mass remains below ~0.08 solar masses, the result is a brown dwarf

Models

- spherical inside-out collapse
- collapse through ambipolar diffusion
- results from numerical MHD
- low mass stars vs. high mass stars
  - (competitive) accretion, protostellar collisions

- the initial, themally supported core being ~λ_J
- in an unstable core, collapse starts from the outside
- in an isothermal core, the collapse results in a steep density profile, ~r^{-2}
  - Larson (1969), Penston (1969)

- mass infall rate ~c_s^2/G
  - applicable even in case of non-thermal support, $c_s^2 \rightarrow c_s^2 + v_{turb}^2 + v_A^2$

Inside-out collapse

- singular isothermal sphere with no thermal support, no magnetic field (spherical symmetry!), no rotation (Shu 1977): start with r^{-2}
- infall region extends inwards on free-fall timescale, after the protostar has formed and the rarefaction wave propagates outwards at sound speed
- more generally, initial condition could be any slightly perturbed hydrostatic solution
- evolution depends on the initial conditions, initially strongly but later only marginally $\frac{dM}{dT} \sim c_s^3/G$
  - e.g., mass accretion rate tends towards or

$$\frac{dM}{dT} \approx 2\times10^{-6} M_{Sun} \left(\frac{T}{10\mathrm{K}}\right)^{3/2} \; yr^{-1}$$

  implying a scales ~0.5Myr for a solar mass protostar

mass infall rate

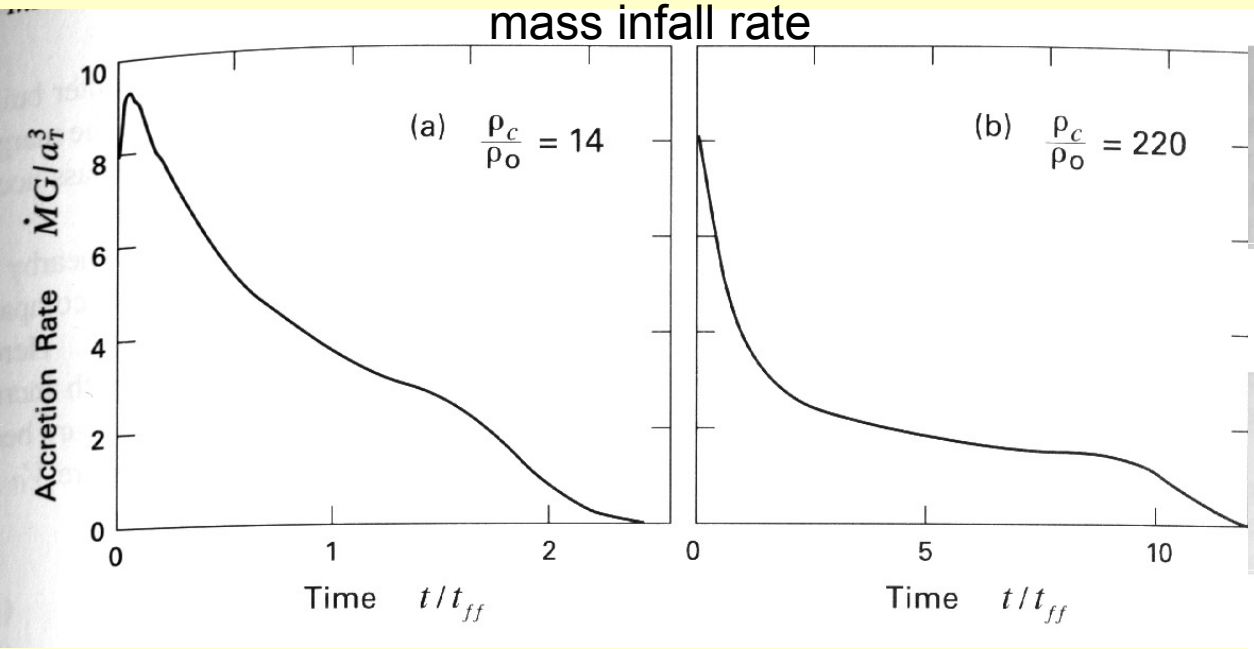

after the formation of the protostar...

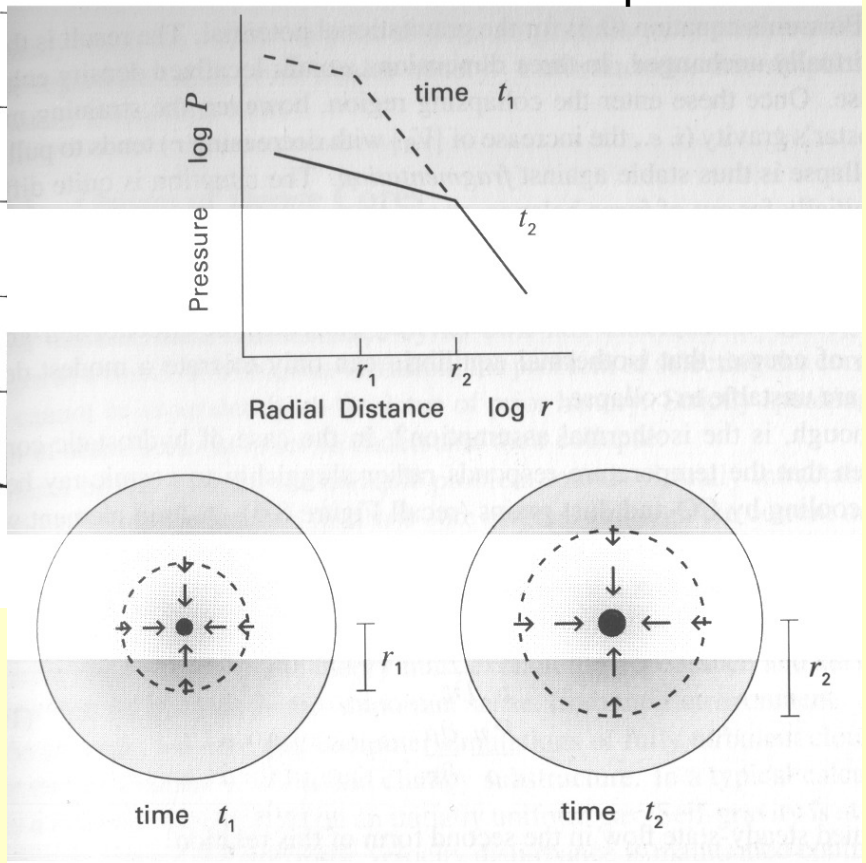

- inner part $n \sim r^{-3/2}$, outer $n \sim r^{-2}$

- for more recent models, see McKee & Ostriker (2007) Sect. 4 and references therein
  - different initial conditions, rotation, turbulence, magnetic fields, etc.

Collapse through AD

- depending on the mass-to-flux ratio, magnetic field can provide significant support against collapse
  - thermal support is strongest in dense parts
  - if field lines follow collapse, M/Φ remains constant
  - ambipolar diffusion can increase M/Φ, especially in dense parts
    - time scale $\tau_{AD} \sim L/v_{drift} = \dfrac{4\pi n n_e \langle \sigma u_i \rangle}{|(\nabla \times B) \times B|}$

      or $\tau_{AD} \approx 1.8 \times 10^6 \left(\dfrac{x_i}{10^{-7}} \right) yr$ (Mouschovias 1979)
  - when drift speed approaches sound speed, the core can continue hydrostatic contraction

Ciolek & Mouschovias (1994)

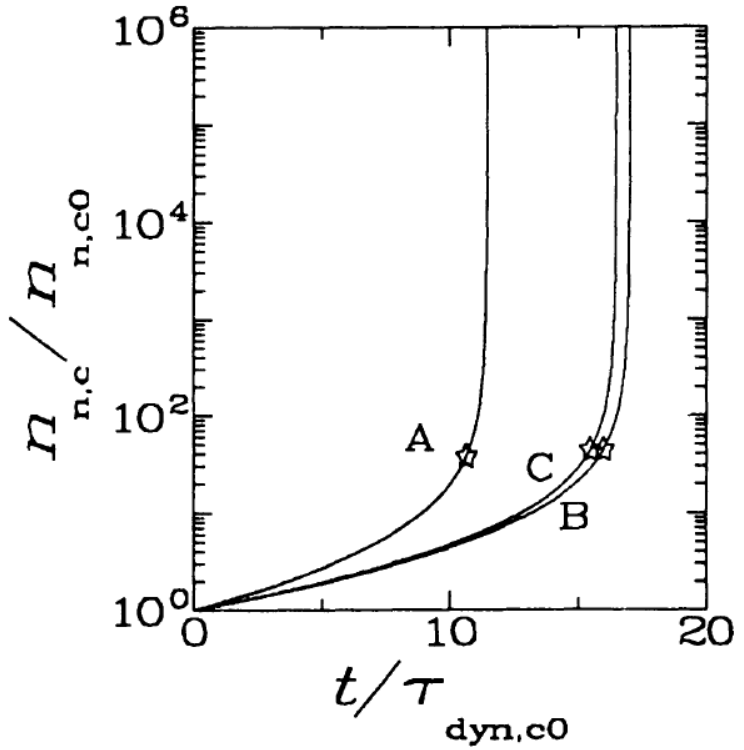

FIG. 1.—Central density $n_{n,c}$ of models A, B, and C normalized to its initial value, $n_{n,c0} = 2.60 \times 10^3$ cm^{-3}, as a function of time t, in units of the initial central dynamical timescale $\tau_{dyn,c0} = 1.07 \times 10^6$ yr. The star on each curve marks the time and density at which the central mass-to-flux ratio becomes equal to the critical value for collapse. Evolution during the subcritical (quasistatic) phase of contraction occurs on essentially the initial central flux-loss time, $\tau_{\Phi,c0} = 11.8$, 17.4, and $16.9\tau_{dyn,c0}$, in models A, B, and C, respectively.

- envelope remains magnetically supported, $n \sim r^{-1.5...-1.9}$
- accretion still controlled by ambipolar diffusion

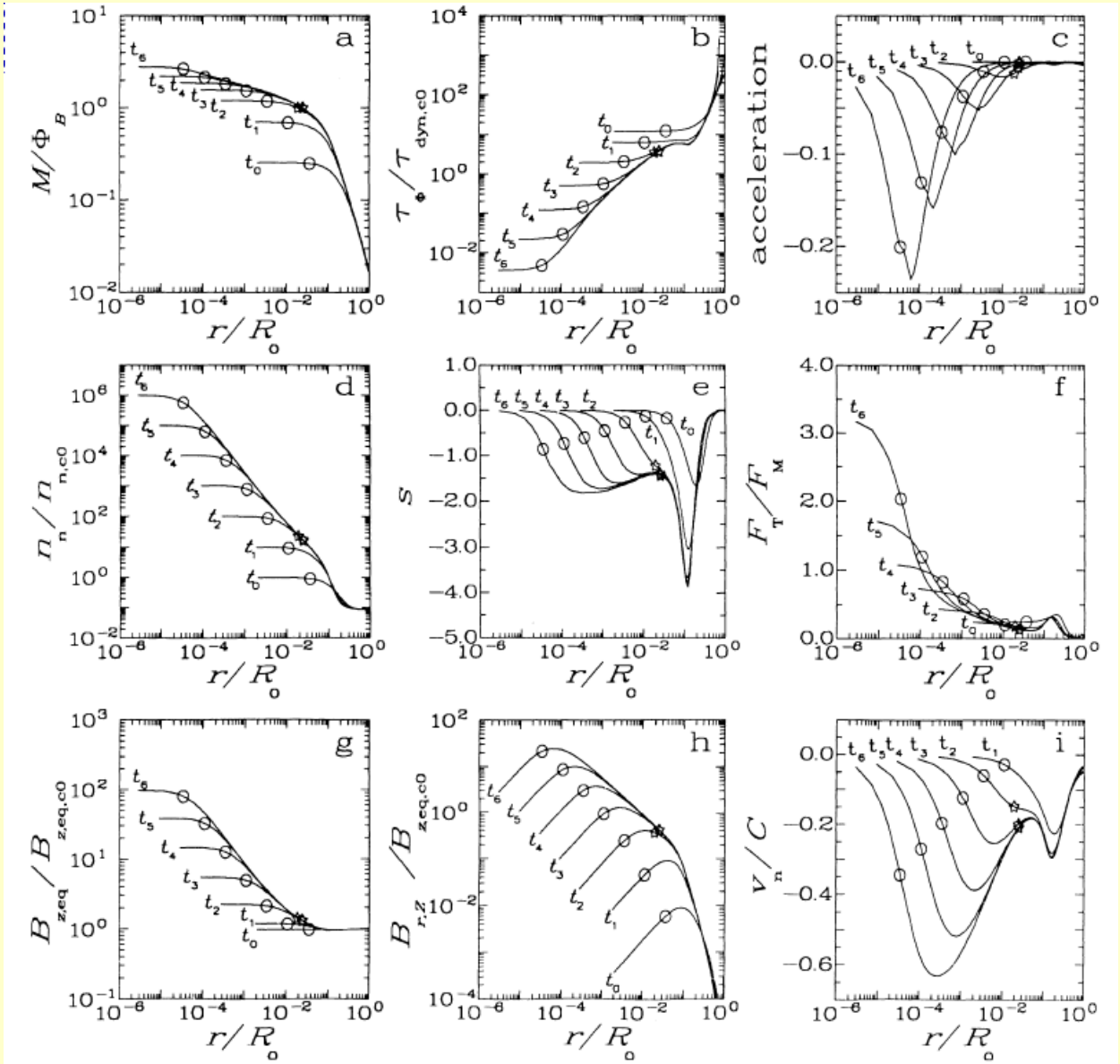

FIG. 3.—Spatial profiles of physical quantities of model A as functions of radius r, normalized to the initial cloud radius R_0 (=4.29 pc), at seven different times t_j ($j = 0, 1, \ldots, 6$) chosen such that the central density at time t_j has increased by a factor 10^j with respect to its initial value. These times are 0, 8.9313, 11.090, 11.385, 11.432, 11.442, and $11.444\tau_{dyn,c0}$. A star on a curve, present only after a supercritical core forms, marks the instantaneous radius of the critical flux tube. An open circle on every curve marks the instantaneous position of the critical thermal length scale. (*a*) Mass-to-flux ratio, normalized to the critical value. Between times t_1 and t_2 a critical core has formed (because of ambipolar diffusion) inside a magnetically subcritical envelope. (*b*) Flux-loss timescale τ_Φ, in units of $\tau_{dyn,c0}$. Because τ_Φ is much greater in the envelope than in the core, the envelope evolves very little during the run. (*c*) Acceleration of the neutrals, normalized to the magnitude of the maximum gravitational acceleration at each time t_j. (*d*) Neutral density, normalized to $n_{n,c0}$. (*e*) The exponent $s \equiv d \ln n_n / d \ln r$. (*f*) Ratio of the thermal-pressure and magnetic forces acting on the neutrals. (*g*) Vertical (z-)component of the magnetic field $B_{z,eq}$ in the equatorial plane, normalized to its initial central value $B_{z,eq,c0}$. (*h*) Radial (r-)component of the magnetic field $B_{r,z}$ at the upper surface of the cloud, normalized to $B_{z,eq,c0}$. (*i*) Infall speed of the neutrals v_n, normalized to the isothermal speed of sound C (=0.188 km s^{-1}). The core loses memory of its initial conditions, and a maximum in the magnitude of the infall speed develops inside the supercritical core at times $t > t_1$. (*j*) Drift speed ($\equiv v_i - v_n$), normalized as in (*i*). Ion-depletion at higher densities is responsible for the maximum appearing in the core (at $r/R_0 \simeq 10^{-4}$) at $t = t_6$. (*k*) Mass infall rate, in units of $M_\odot$ Myr^{-1}. It decreases from its maximum by more than two orders of magnitude in the magnetically supported envelope.

- ambipolar diffusion allows mass to slowly accrete without dragging all field lines with it
- because of magnetic reconnection, the final rapid collapse will not necessarily drag field lines to the protostar
- at still later stages, Ohmic dissipation may become important (=high densities)

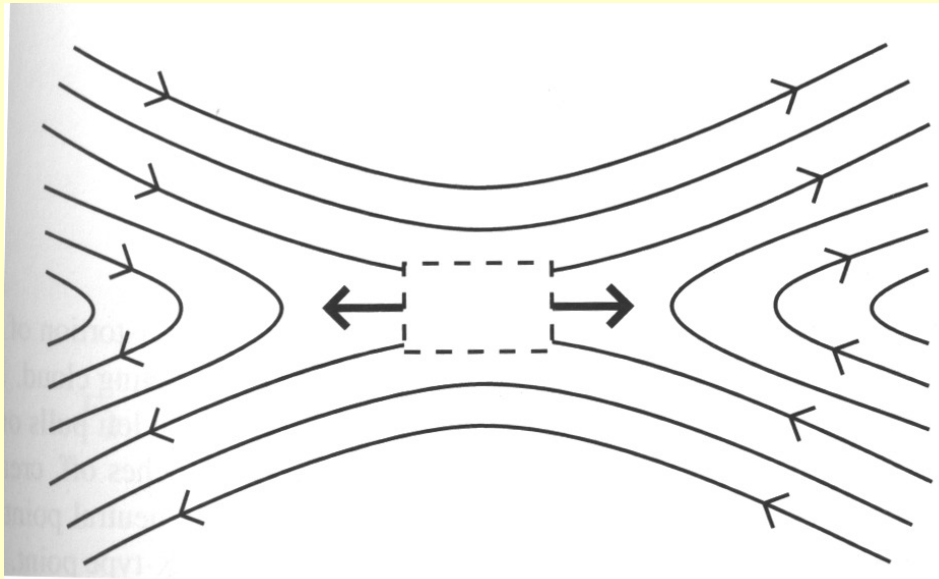

Figure 10.10 Topology of magnetic reconnection (*schematic*). Field lines of opposite direction press together, creating a small region (*dashed rectangle*) of high Ohmic dissipation. Pressure on this region expels fluid laterally, as indicated.

Stahler & Palla, Sect. 10

Angular momentum

- clouds always contain motions that, when amplified by the collapse over a range of scales ~10^5, cause rapid rotation
  - in cylinder geometry, centrifugal force increases as r^{-3} while graviation increases only as r^{-2}
  - the existence of accretion disks shows that angular momentum is a problem for accretion
  - the angular momentum problem affects time scales but does not eventually stop star formation

the reasoning (e.g. Lodato 2008)

- typical values given by Jeans length and Jeans mass

$$L_J = \frac{2\pi c_s}{\sqrt{4\pi G\rho}}, \quad M_J = \rho L_J^3 = \left(\frac{\pi}{G}\right)^{3/2} c_s^3 \rho^{-1/2}$$

- for T=10K and μ=2.3, Jeans length is ~0.1pc for a one solar mass core
- estimate for a typical angular momentum is

$$j \approx \Omega_{core} L_J^2 \approx 10^{21} - 10^{22} \ cm^2 s^{-1}$$

- infalling material should end up at a Keplerian orbit where $j_K = \sqrt{GMR}$
- this implies radiae for one solar mass star

$$R_{disk} = \frac{j^2}{GM} \approx 10^2 - 10^4 \ AU$$

- how to lose angular momentum?
  - direct magnetic breaking $F_\phi = \frac{1}{4\pi}\left[(\nabla \times B)\nabla B\right]_\phi$
    - protostar is connected to its surroundings through magnetic field which exerts a breaking force
  - the understanding of breaking and the loss of angular momentum requires understanding of disks and outflows
  - obviously angular momentum is lost, because accretion rates are non-negligible
    - from 10^{-11} solar masses per year in brown dwarfs to 10^{-9} to 10^{-7} in normal T Tauri stars and up to 10^{-5} solar masses per year in massive stars

Stahler & Palla

Accretion disk

- conservation of angular momentum leads to flattened structure around the protostar
  - found probably around all protostars although information on massive stars is still incomplete
  - accretion disk = material is accreted onto the disk, transported inwards, fed into the protostar
  - the shape is dictated by the accretion flow and the balance between gravitation, rotation, thermal pressure, and magnetic fields
  - sizes from ~1000 AU (molecular) to ~10AU (visible)
  - start by considering them as static systems...


Edge-On Protoplanetary Disk
Orion Nebula
PRC95-45c · ST ScI OPO · November 20, 1995
M. J. McCaughrean (MPIA), C. R. O'Dell (Rice University), NASA
HST · WFPC2

- Keplerian disk $v = \sqrt{\frac{G M}{r}}$
- gravitational potential dominated by the central mass, disk is not massive and is rather thin
- assuming the disk is heated by radiation from the central object, temperature profile is expected to be a powerlaw
  - according to Stahler & Palla (p. 656) for *thin* but *optically thick* disk $T \approx \left(\frac{2}{3\pi}\right)^{1/4} \left(R_{star}/R\right)^{3/4} T_{eff}$
  - in observations, the temperature profile is not quite as steep

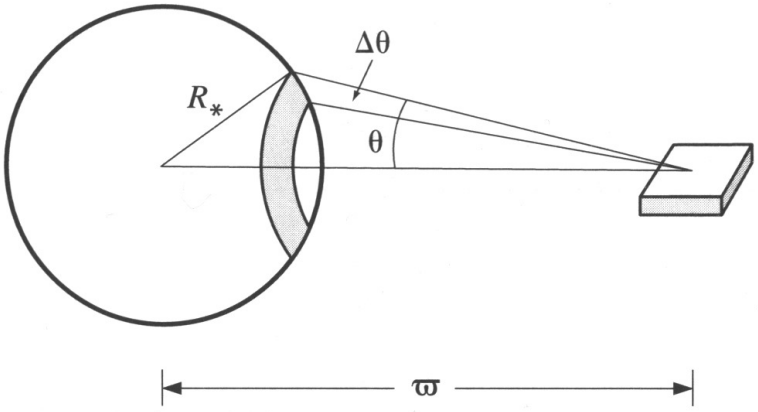

Figure 17.17 Irradiation of a disk patch by a spherical star.

$$\Delta F = f_\theta \Delta \Omega \int B(\lambda)\, d\lambda$$

$$\Delta \Omega = \pi \sin\theta \, \Delta\theta$$

$$f_\theta = \langle grazing\ angle \rangle = \frac{2}{\pi} \sin\theta$$

$$F_{in} \approx \frac{2}{3\pi} \sigma_B T_{eff}^4 \left(\frac{R_{star}}{r} \right)^3$$

$$F_{in} = F_{out} \approx \sigma T_{dust}^4$$

$$\Rightarrow$$

$$T = \left(\frac{2}{3\pi} \right)^{1/4} \left(\frac{R_{star}}{r} \right)^{3/4} T_{eff}$$

- Flared disk
  - assuming gravitational potential is dominated by the central object, vertical balance requires

$$\frac{1}{\rho}\frac{\partial P}{\partial z} = -\frac{d\Phi}{dz} \quad \Rightarrow \quad \frac{\partial P}{\partial z} = -\rho G M_* \frac{z}{r^3}$$

    which leads to a result that disk scale height depends on temperature and radius

$$\Delta z \approx c_s \frac{r}{v} \propto T^{1/2} r^{3/2} \quad (c_s \propto T^{1/2}, \quad v \propto r^{-1/2})$$

  - the central object can illuminate full surface
  - the grazing angle is $\theta \propto T^{1/2} r^{3/2}$, and the flux on the surface is proportional to θ / r^2
  - the temperature (still assuming an optically thick disk) is

$$T \propto \left(\frac{\theta}{r^2} \right)^{1/4}$$

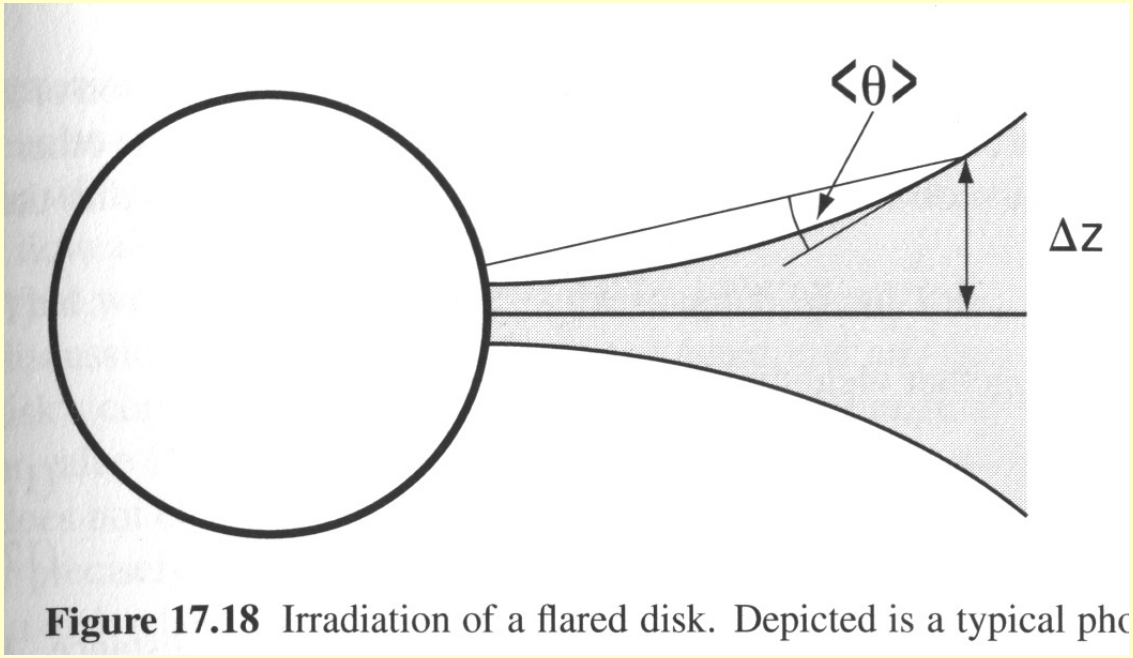

Figure 17.18 Irradiation of a flared disk. Depicted is a typical pho

- calculating grazing angles consistently with the radial temperature profile results in relations

$$\theta \propto r^{2/7}, \quad T \propto r^{-3/7}$$

- the flaring has obvious consequences, not only for thermal dust emission but also lines observable in the outer disk
  - one should also take into account vertical temperature gradient, heating in the disk, convection, finite optical depths, photoevaporation etc.

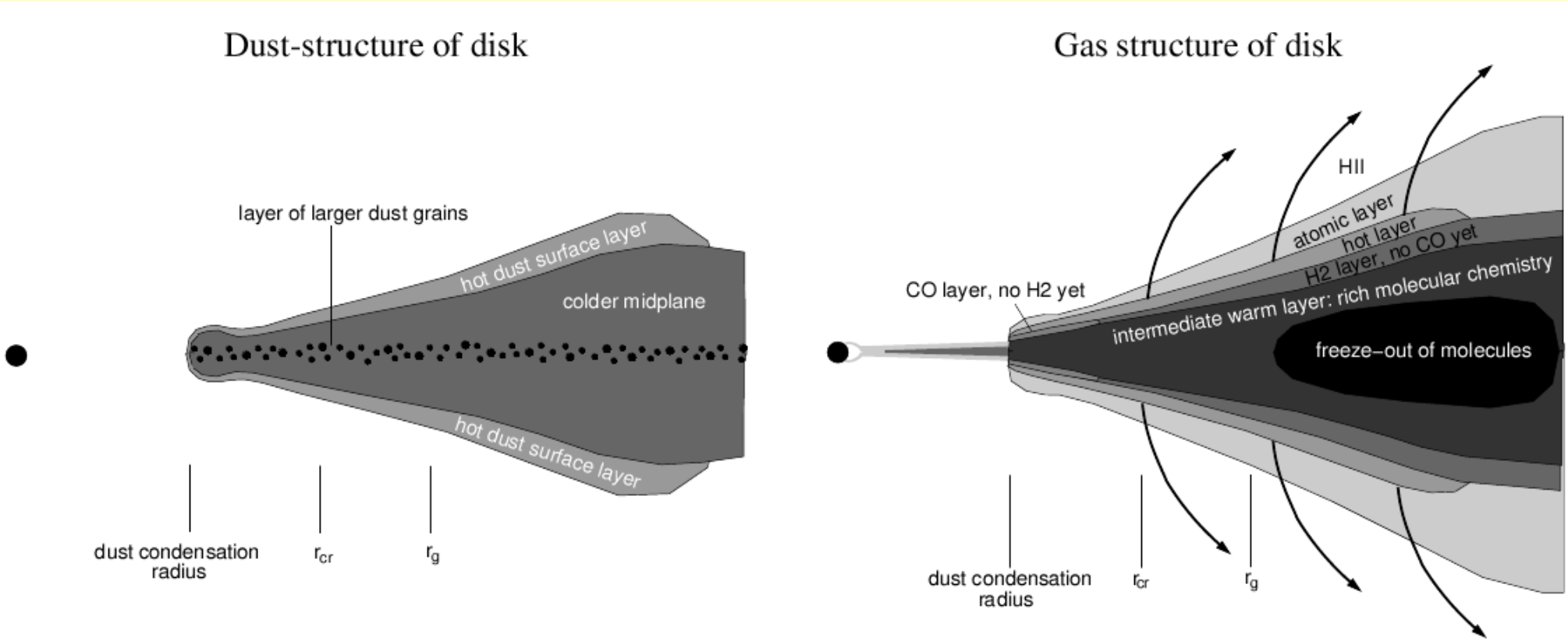

Fig. 13.— Pictograms of the structure of a flaring protoplanetary disk, in dust (left) and gas (right).

Dullemond et al. (2007)

Ramos, Ceccarelli, Elitzur (2007)

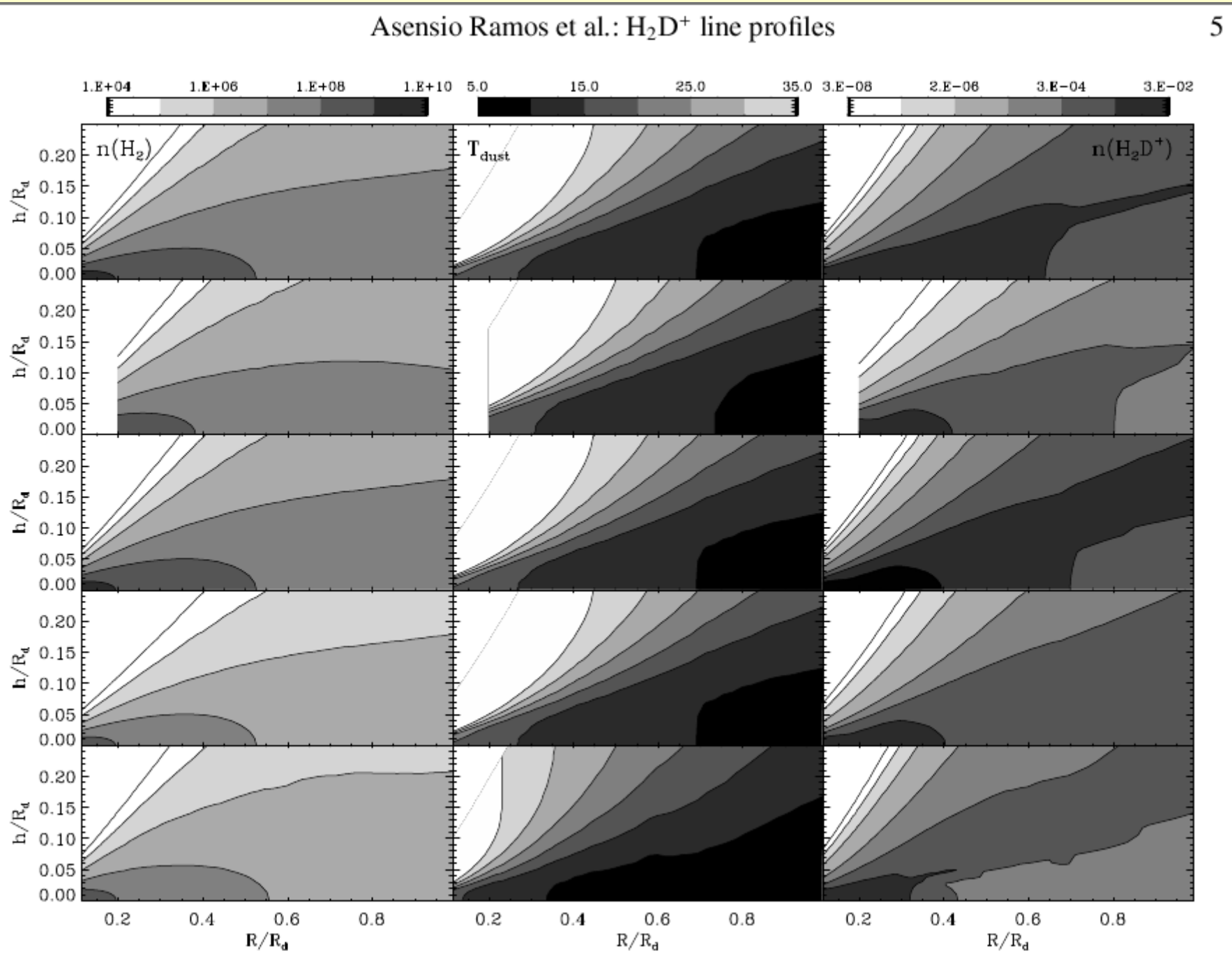

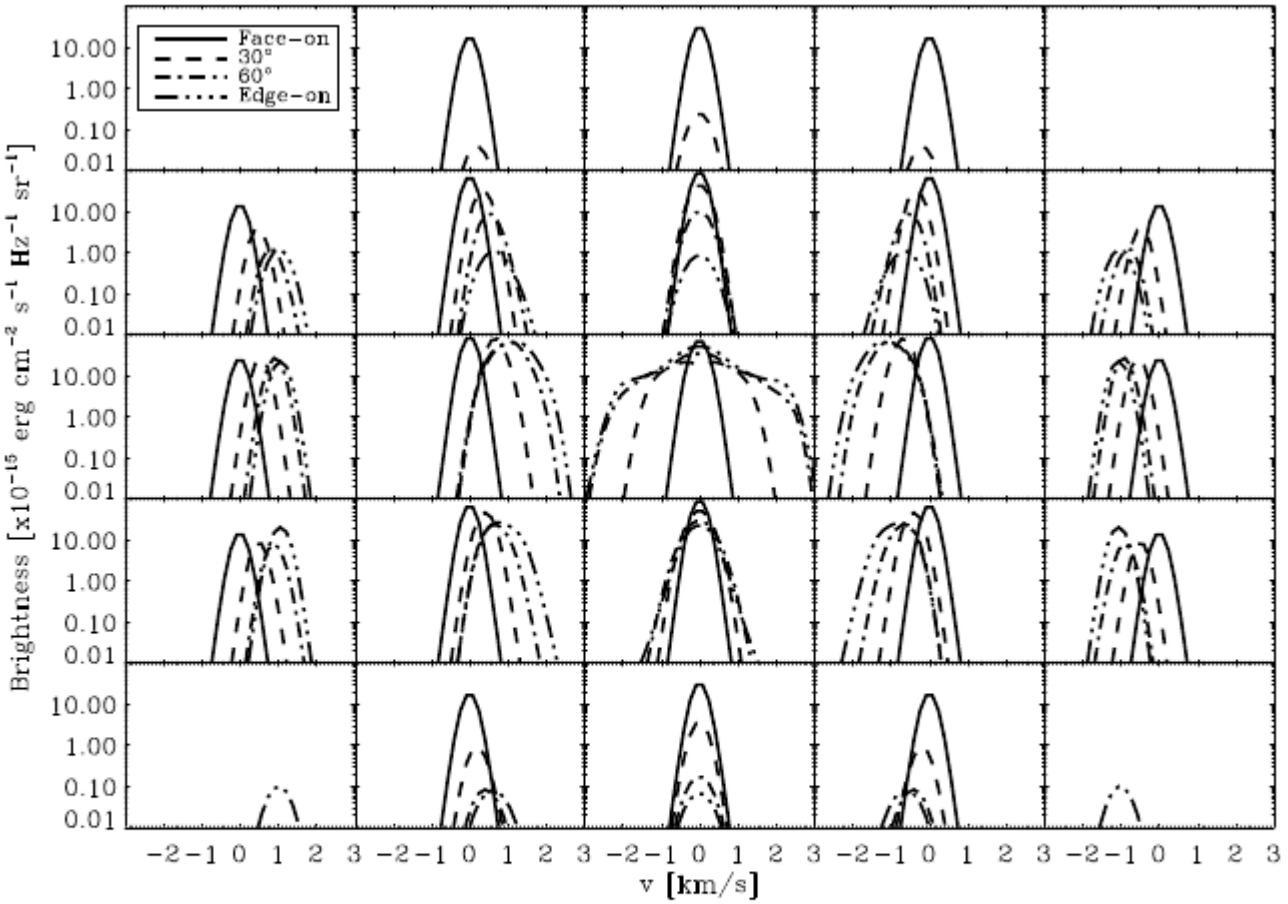

Fig. 6. Variation of line profile across the disk image for Model 1 at various inclinations, as marked. The displayed mosaic is centered on the disk image and was produced as follows: The maps shown in figure 4 are divided into grids of 5×5 squares, each with 1.2″ on the side. At a given velocity, the brightness is averaged over each square with a Gaussian beam of 0.3″, the ALMA beam size.

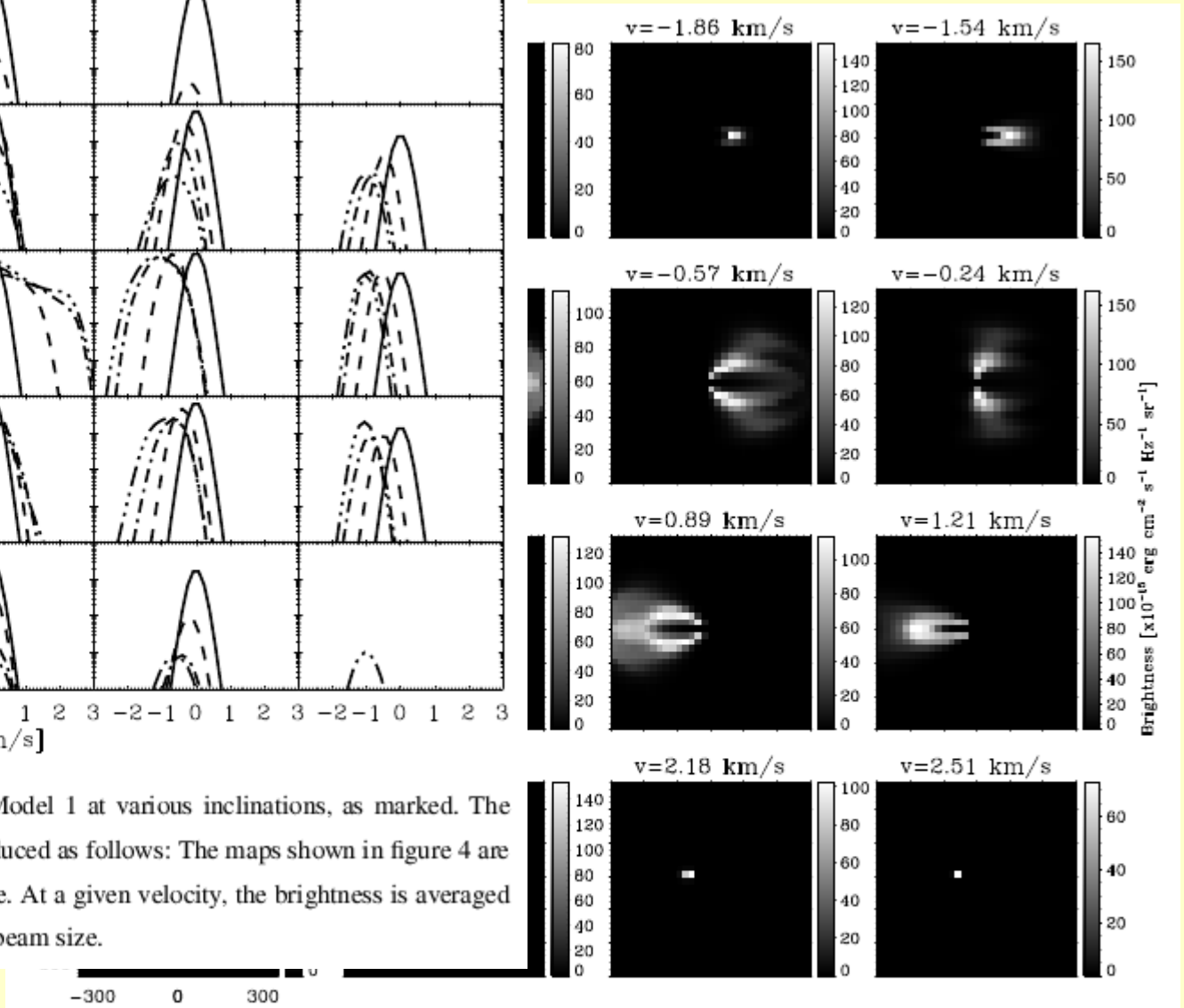

Fig. 5. Channel maps of the H_2D^+ line intensity (convolved with ALMA beam; see Fig. 4) for the standard disk (Model 1), viewed at an inclination of 30°. The x and y axes are displacements, in AU, from the disk center. The central velocity of each map is marked on top. The bar to the right of each panel shows the contour brightness scale. Note the scale changes among the panels.

role of viscosity (see Lodato 2008)

- start with equation of motion and continuity

$$\frac{\partial v}{\partial t}+(v\cdot\nabla)v \;=\; -\frac{1}{\rho}(\nabla P-\nabla\cdot\sigma)-\nabla\phi$$

$$\frac{\partial \Sigma}{\partial t}+\frac{1}{R}\frac{\partial}{\partial R}\left(R\Sigma v_R\right) \;=\; 0$$

- in cylinder coordinates, using vertically integrated stress tensor components T, the equation for the ϕ-component becomes

$$\Sigma\left(\frac{\partial v_\phi}{\partial t}+\frac{v_R v_\phi}{R}+v_R\frac{\partial v_\phi}{\partial R}\right) \;=\; \frac{1}{R^2}\frac{\partial}{\partial R}\left(R^2 T_{R\phi}\right)$$

- with continuity equation, this can be rewritten

$$\frac{\partial}{\partial t}\left(\Sigma R v_\phi\right)+\frac{1}{R}\frac{\partial}{\partial R}\left(R v_R \Sigma R v_\phi\right) = \frac{1}{R}\frac{\partial}{\partial R}\left(R^2 T_{R\phi}\right)$$

  - left side = Lagrangian derivative of angular momentum per mass
  - right side = torque exerted by viscous forces

- for Keplerian rotation

$$v_\phi = \sqrt{GM/R}, \quad \Omega = v_\phi/R = \sqrt{GM/R^3}, \quad R v_\phi = \sqrt{GMR}$$

- assume further a simple shear viscosity

$$\sigma_{R\phi} = \rho \underline{\nu} R \frac{d\Omega}{dR}$$

- in this simple case

$$\frac{\partial}{\partial t}\left(\Sigma R^2 \Omega\right)+\frac{1}{R}\frac{\partial}{\partial R}\left(\Sigma v_R R^3 \Omega\right) = \frac{1}{R}\frac{\partial}{\partial R}\left(\nu \Sigma R^3 Q'\right)$$

- using again the continuity equation, one can solve radial velocity

$$v_R = \frac{\partial}{\partial R}\left(\nu \Sigma R^3 Q'\right) / \left(R\Sigma \frac{\partial}{\partial dR}\left(R v_\phi\right)\right) = -\frac{3}{\Sigma R^{1/2}}\frac{\partial}{\partial R}\left(\nu \Sigma R^{1/2}\right)$$

and get an equation for surface density

$$\frac{\partial \Sigma}{\partial t} = \frac{3}{R}\frac{\partial}{\partial R}\left[R^{1/2}\frac{\partial}{\partial R}\left(\nu \Sigma R^{1/2}\right)\right]$$

- diffusion equation, disk evolution dictated by viscosity

- see Lodato (2008), Shu et al. (2007)

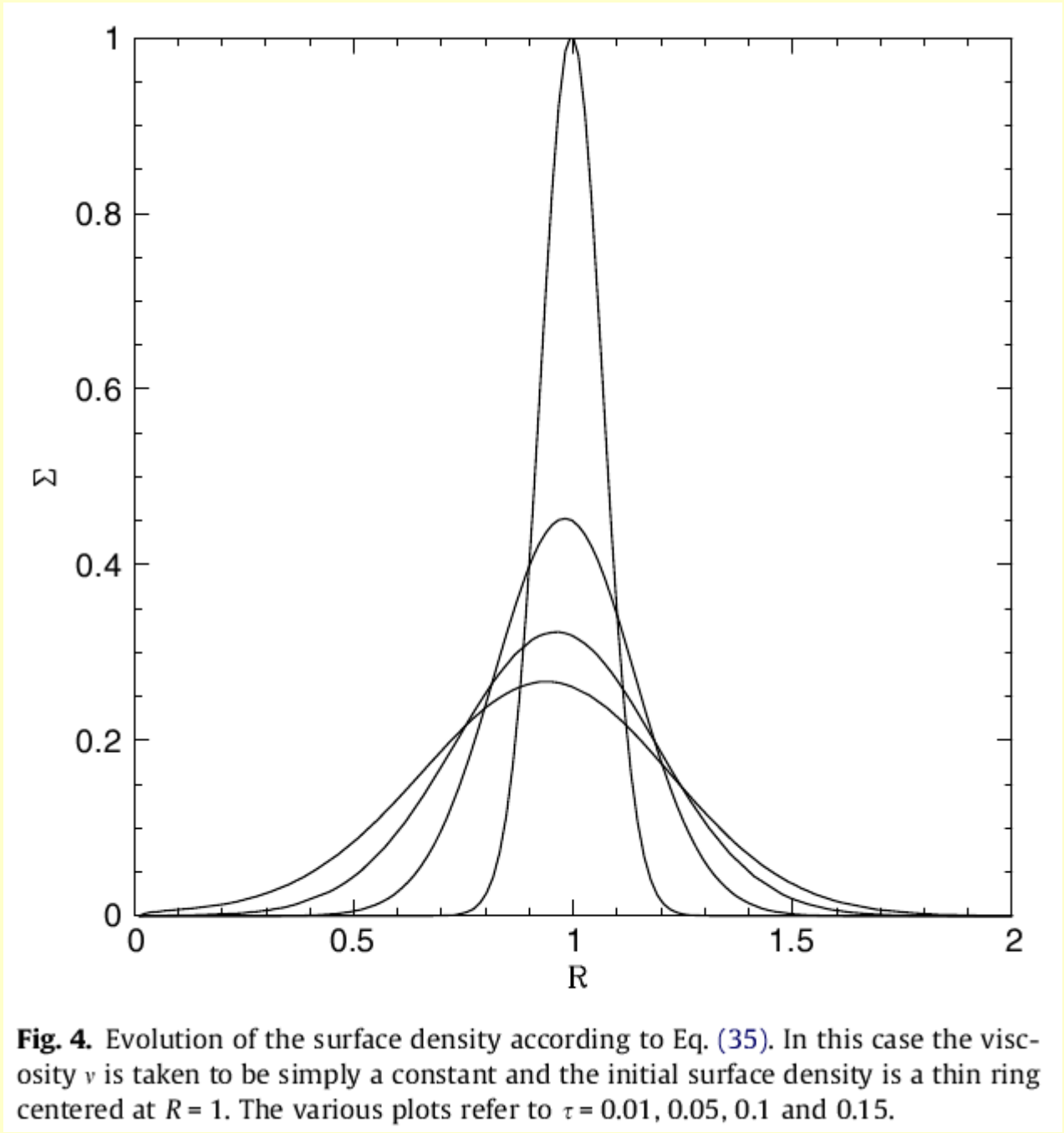

Fig. 4. Evolution of the surface density according to Eq. (35). In this case the viscosity ν is taken to be simply a constant and the initial surface density is a thin ring centered at $R = 1$. The various plots refer to $\tau = 0.01, 0.05, 0.1$ and 0.15.

Lodato (2008)

- the accretion rate onto protostar can be parametrisized with an parameter α, (Shakura & Sunyaev 1973) where Q is 'instability parameter'

$$\dot{M}_* = \frac{3\alpha c_s^3}{GQ}$$

$$Q = \frac{c_s \kappa}{\pi G \Sigma}$$

- the rate depends on at least two processes

$$\alpha \sim \alpha_{GI} + \alpha_{MRI}$$

  - Gravitational Instability: if a volume element is compressed, increased gravity may overcome pressure terms and disk is instable (*Q*~1 or below in the above equation)
    - asymmetry, spiral patterns, eventually fragmentation
  - Magneto-Rotational Instability: a field line gets extruded together with a perturbed volume element: constant Ω → larger centrifugal force

- also thermal instabilities: higher temperature implies higher heating

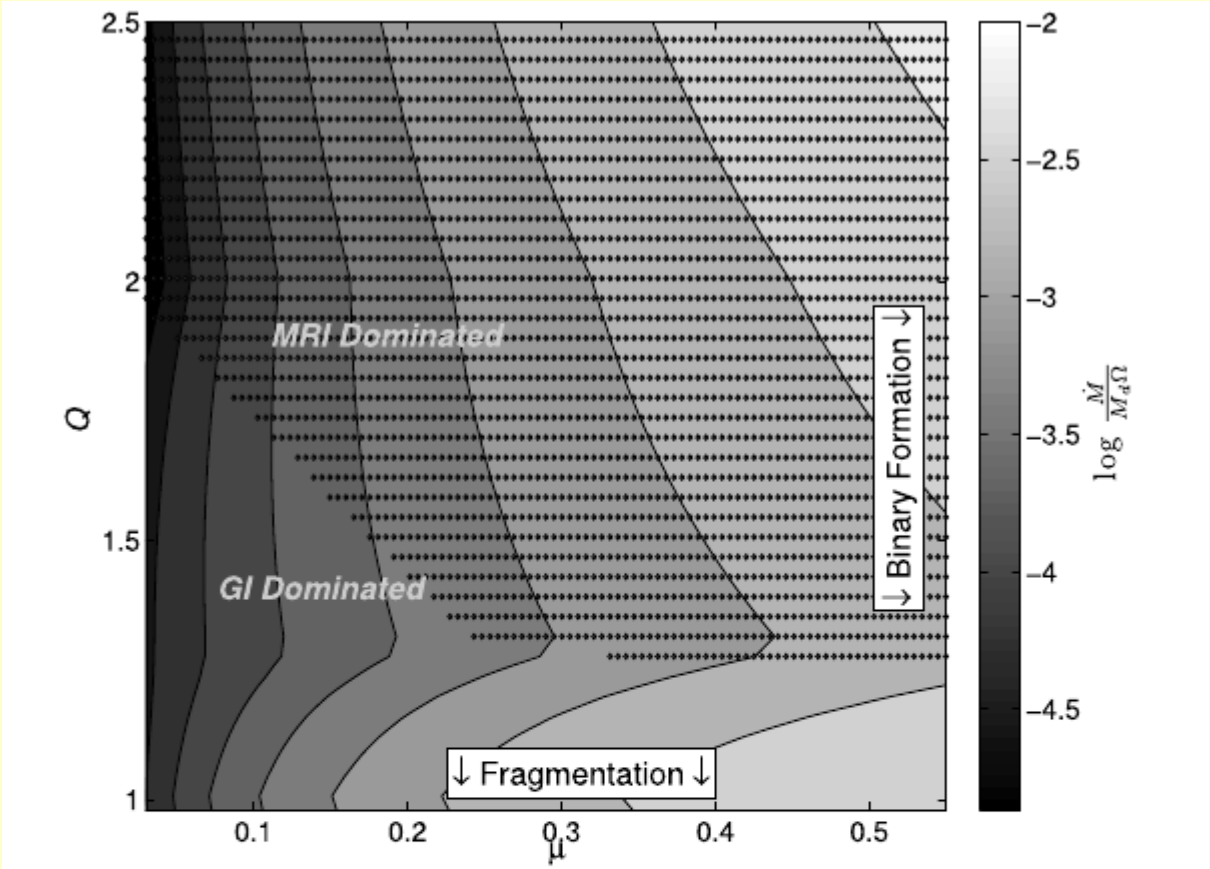

FIG. 2.—Contours of the dimensionless accretion rate $\dot{M}_*/(M_d\Omega)$ from the disk onto the star from all transport components of our model. The lowest contour level is $10^{-4.8}$, and subsequent contours increase by 0.3 dex. The effect of each transport mechanism is apparent in the curvature of the contours. At $Q < 1.3$ the horizontal "tongue" outlines the region in which short-wavelength instability dominates accretion. The more vertical slope of the contours at lower μ and $Q > 1.3$ shows the dominance of the long-wavelength instability. The MRI causes a mild kink in the contours across the $Q = 2$ boundary and is more dominant at higher disk masses due to our assumption of a constant α: eq. (13) illustrates that a constant α will cause higher accretion rates at higher values of μ. [*See the electronic edition of the Journal for a color version of this figure.*]

$$\mu = \frac{M_{disk}}{M_{star} + M_{disk}}$$

Kratter et al. (2008)

Outflows

- like disks, an integral part of the protostar phase
  - bipolar outflows common to all accreting systems
  - inner ionized jet (velocities ~10 to ~100 km/s) and more massive neutral/molecular outflows (velocities ~10km/s or less)
  - well collimated (age dependent)
  - the jets exhibit internal shocks, bow shocks are observed when outflow collides with the ambient medium
    - needs several tracers: xrays, visual lines, NIR lines (H_2, [FeII]), infrared emission, radio lines...

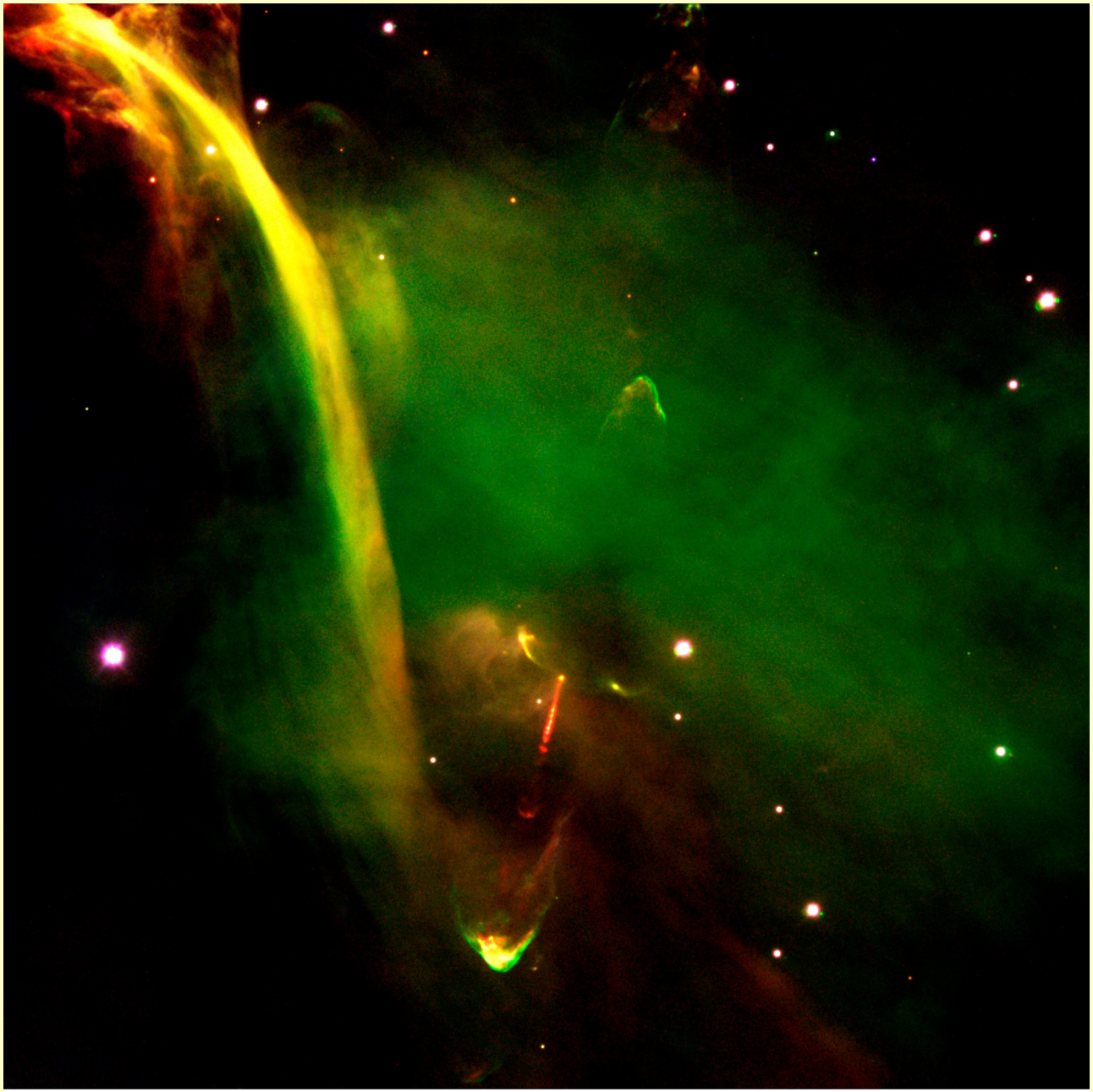

Protostar HH-34 in Orion (VLT KUEYEN + FORS2)

ESO PR Photo 40b/99 (17 November 1999)

- outflows
  - drive turbulence in the ISM and shock chemistry within outflow region (e.g. SiO, H_2O)
  - clear outflow cavities (visible as polarized scattered radiation) and eventually the protostellar envelopes
  - transfer angular momentum from the protostar

- questions
  - does outflow originate in disk, in protostar (or in between)?
  - how is the outflow actually driven?
  - how is the outflow collimated?

- radiation pressure is not sufficient to drive outflows
- there exist two main MHD wind models
  - x-wind model
    - wind starts at the interaction region of the stellar magnetosphere and the inner disk
    - stellar field concentrated close to the star where the disk co-rotates; terminal velocities ~100km/s possible
  - disk wind models
    - larger region of the disk is threaded by the field that could be partially locally generated
    - outflow velocity varies depending on the point of origin
  - same mechanism, only point of origin differs
    - ” magnetorotational launching”

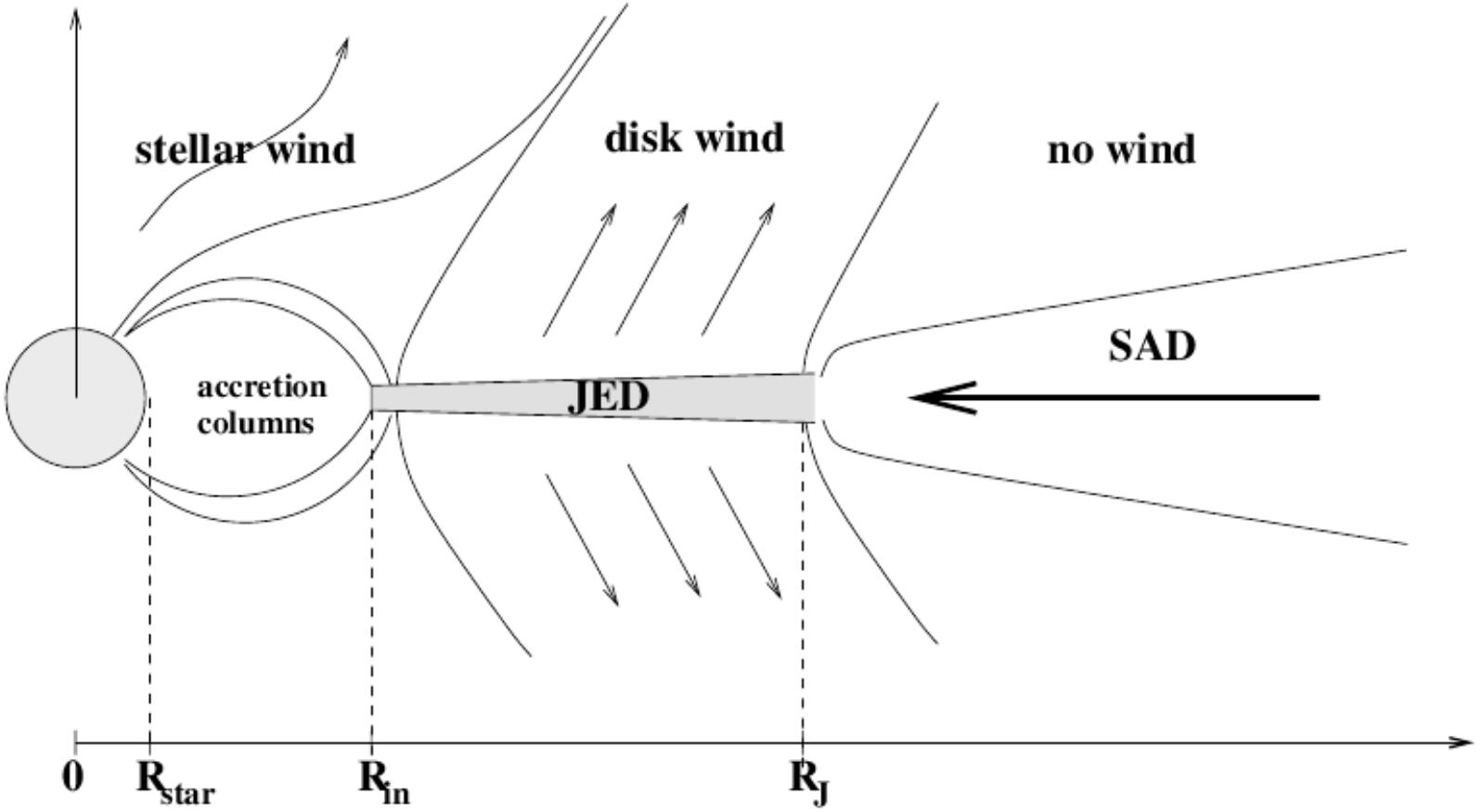

Fig. 1. Sketch of the accretion configuration suggested in this work. The accretion disk is constituted by a SAD in the outer part whereas the inner part is occupied by a JED. See text for details. Accretion columns onto the central object and a possible stellar wind are also represented, although they are not considered in the study.

Combet et al. (2008)

consider outflow along magnetic field lines (see, e.g., Pudritz et al. 2007)

- mass and magnetic flux are conserved along a field line → the *mass load* remains constant

$$k = \frac{\rho v_p}{B_p} = \frac{d\dot{M}}{d\Psi} = const.$$

- the toroidal field depends (through induction equation) $B_\phi = \frac{\rho}{k}\left(v_\phi - \Omega_0 r\right)$ but, because high mass load means dense wind, high mass load does correlate with strong field toroidal field
- conservation of angular momentum involves both mass and magnetic field

$$r v_\phi - \frac{r B_\phi}{4\pi k} = const.$$

  - relative contributions depend on mass load

- the mass follows the field up to a point, where the outflow velocity exceeds Alfven velocity

$$L = \Omega_0 r_A^2 \Rightarrow L/L_0 = \left(r_A/r_0\right)^2 \gg 1$$

  - the angular momentum is $(r_A/r_0)^2$ times the original angular momentum within the disk

- based on energy conservation, one can estimate the final velocity $v_\infty = v_{escape} \frac{r_A}{r_0} \gg v_{escape}$

  - can drive high speed ouflows; inner flow will have higher velocity

- one can also derive a relation between accretion and outflow rates $\frac{\dot{M}_{wind}}{\dot{M}_{accretion}} = \left(\frac{r_0}{r_A}\right)^2$

  - see Königl & Pudritz 2000
  - observationally the ratio is ~0.1, consistent with $r_A/r_0 \sim 3$

- beyond the Alfven surface, field is mainly toroidal

$$B_\phi / B_p = r / r_A$$

and the Lorentz force exerts a pinch $F = j_z B_\phi$

- the degree of collimation varies depending on the mass loading
  - can explain both tightly collimated jets and wide angle winds; however, collimation does not work in all situations
  - dynamo action may produce magnetic fields that drive outflows but strong collimation seems to require ambient field

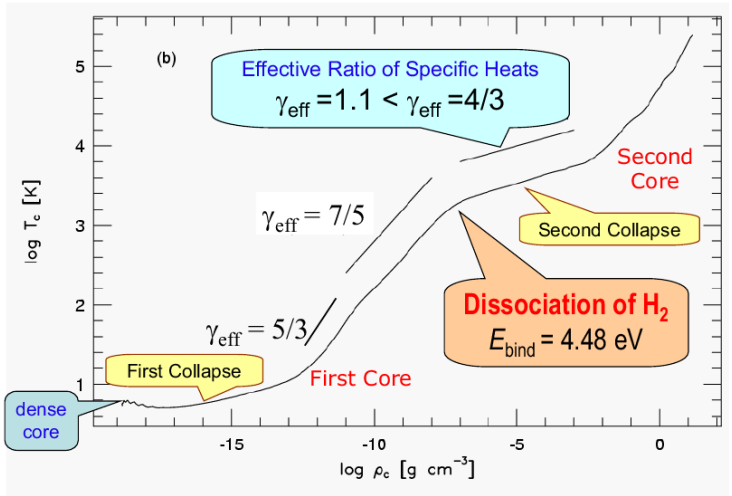

Figure 9. Temperature evolution at the center of a gravitationally collapsing cloud obtained by Masunaga & Inutsuka (2000a) in their radiation hydrodynamical calculation of protostellar collapse in spherical symmetry. The *first collapse* phase corresponds to the formation of the *first protostellar core* that consists mainly of hydrogen molecules. The dissociation of hydrogen molecule triggers the *second collapse* that eventually produces the *second core*, i.e., a protostellar object. Each of these phases in the temperature evolution is characterized by a distinct value of the effective ratio of specific heats, γ_{eff}.

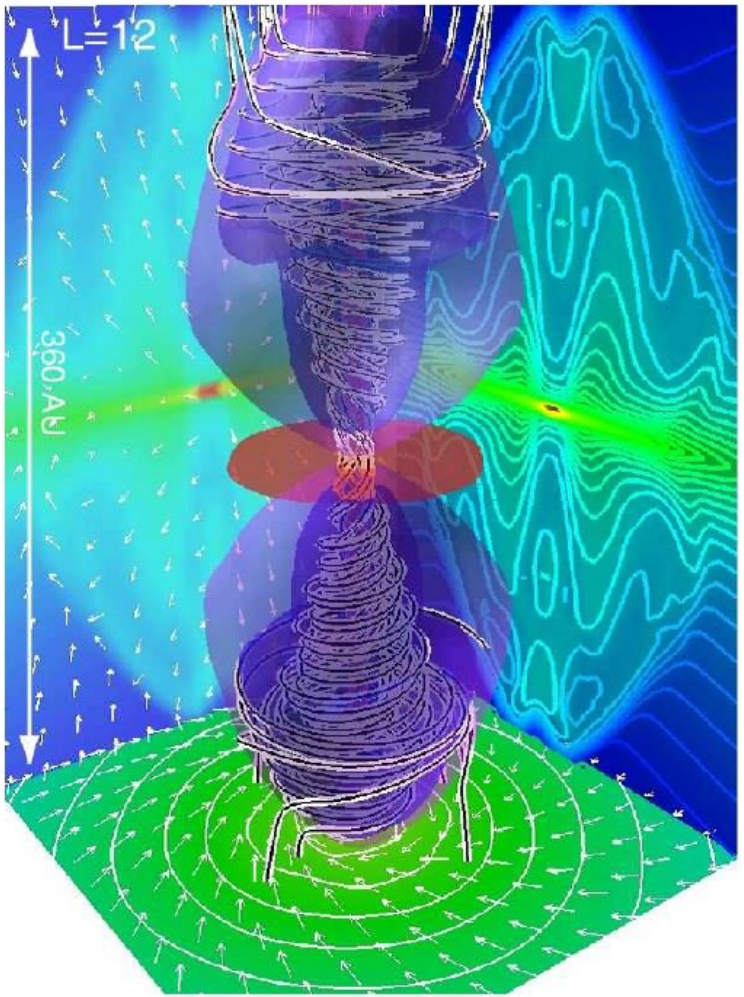

Figure 10. Bird's-eye view of model RR ($l = 12$). The structure of high-density region ($n > 10^{12}$ cm^{-3}; iso-density surface), and magnetic field lines (black-and-white streamlines) are plotted. The structure of the outflow is shown by the iso-velocity surface inside which the gas is outflowing from the center. The density contours and velocity vectors (thin arrows) on the mid-plane of $x = 0$, $y = 0$, and $z = 0$ are, respectively, projected in each wall surface.

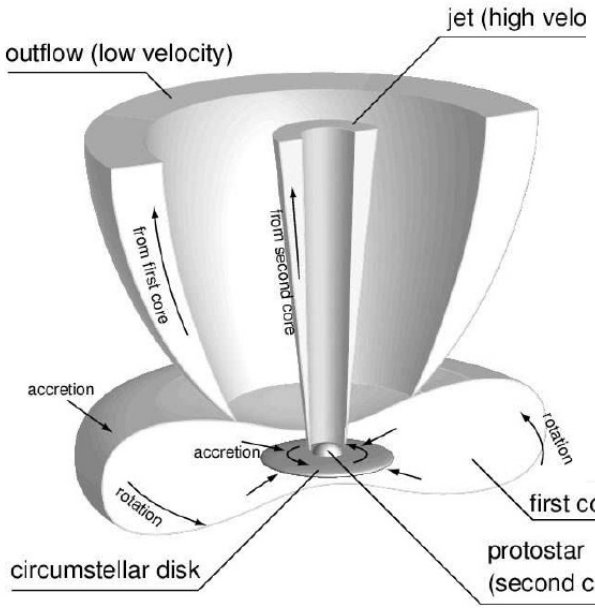

Figure 11. Schematic picture proposed by Machida et al. (2007b) for the jet and outflow driven from the protostar and the fist core, respectively.

Andre et al. (2008)

Machida (2007)

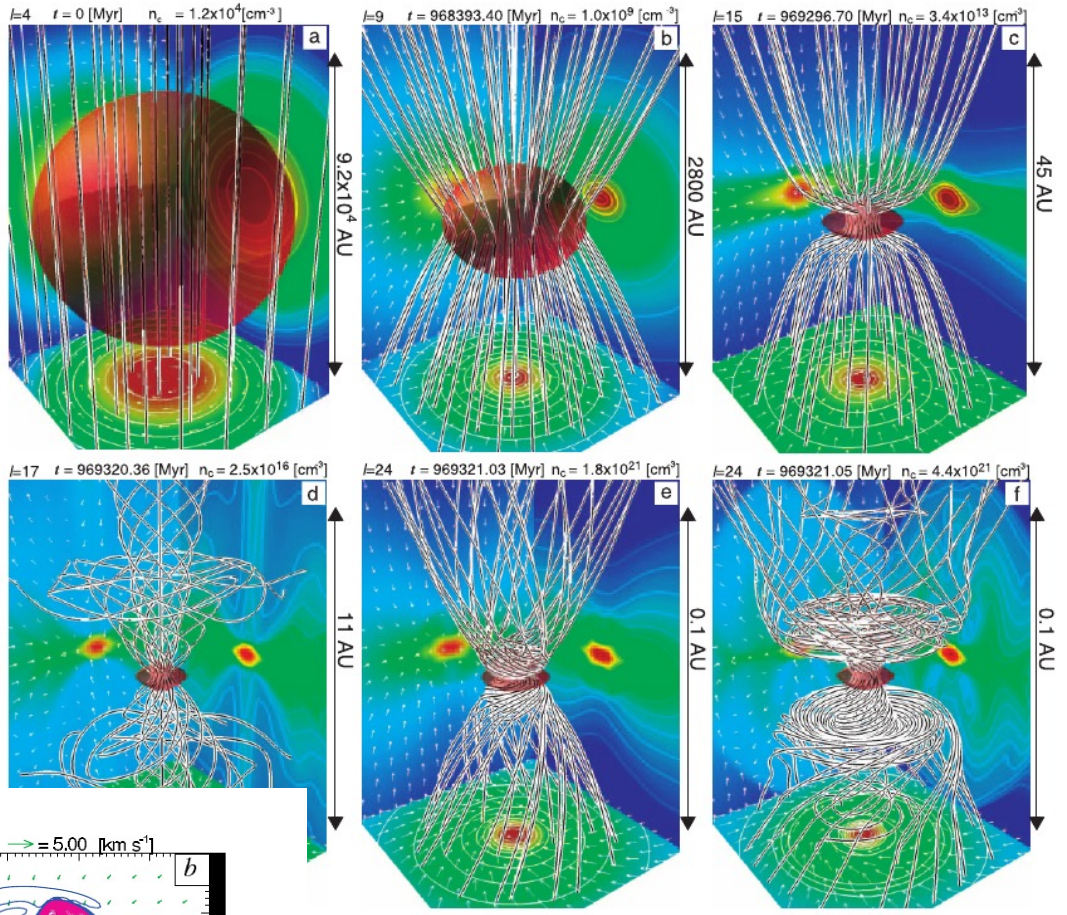

anels (a–f) have the same scale and epoch as panels (a–f) of Fig. 4. The structure of the high-density region lines (*black-and-white streamlines*) are plotted in each panel. The density contours (*false color and contour* s in the $x = 0$, $y = 0$, and $z = 0$ planes are, respectively, projected on the sidewalls of the graphs. The grid level, l, are denoted in each panel.

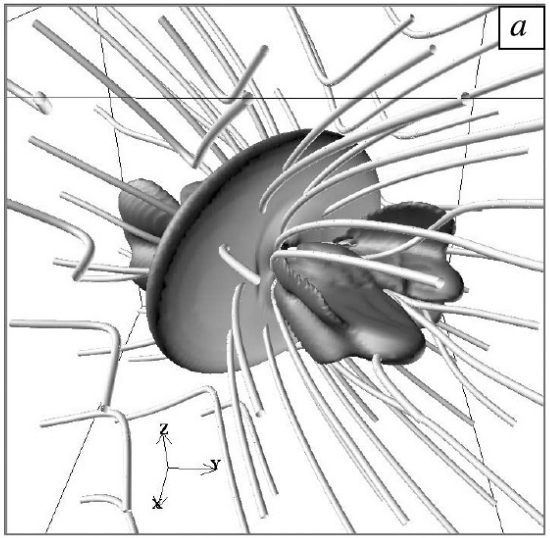

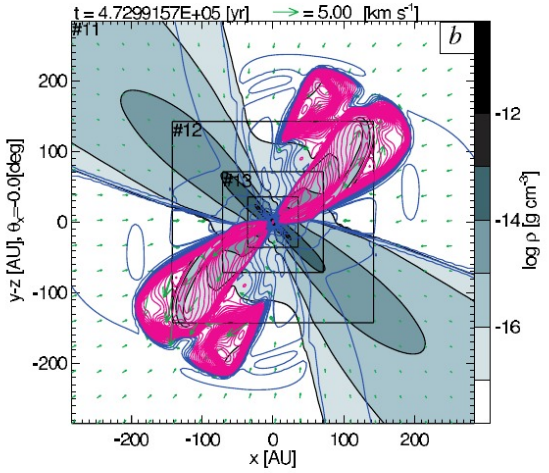

FIG. 8.—Density, velocity, and magnetic field distributions for model MF90. (a) Three-dimensional structure of the outflow region at $t - t_c = 464$ yr, where the outflow speed reaches its maximum of 6.14 km s^{-1}. Streamlines denote the magnetic field lines, and the disklike surface represents the isodensity surface of $10^5\rho_0$. Other surfaces denote the isovelocity surfaces of $v_r = c_s$. Box size is 287 AU ($l = 12$). (b) Cross section of outflow region in the final stage using the same notation as Fig. 1.

Matsumoto (2004)

Massive stars

- massive star formation differs from low mass star formation at least because of the higher radiation pressure and strong photoionization
- some ideas on the formation mechanism
  - competitive accretion / turbulent core formation
    - continued accretion; radiation pressure problem solved by removing spherical symmetry
    - strong radiation from protostar prevents further core fragmentation
  - collisions of lower mass protostars
    - possible in dense clusters through star-disk interactions
    - massive stars found preferentially in the centre of the clusters?

Accretion luminosity

- assume initial energy of the system is zero
- in final protostar, thermal energy is $U=-W/2$ (virial theorem), and $W=-GM^2/R_{\rm star}$

$$0 = -\frac{1}{2}\frac{G M^2}{R_{star}} + \Delta E_{int} + L_{rad} t$$

  - second term = dissociation and ionization of H and He
  - third term = energy radiated during collapse
- radiated energy $L_{\rm rad}$ is close to accretion luminosity

$$L_{acc} \equiv \frac{G M \dot{M}}{R_{star}}$$

  - = radiation power assuming all kinetic energy is transformed into radiation

Radiation pressure (McKee & Ostriker 2007, Sect. 4.3.3)

- if the protostar is massive enough, its radiation pressure should be sufficient to stop accretion
- stellar luminosity should equal Eddington luminosity

$$L_{ed} = \frac{4\pi c G M}{\kappa_d}$$

- equation involves dust opacity (per unit mass) because that is the main source of opacity for non-ionizing radiation; $\kappa \sim 8$ cm^2 g^{-1} or less
- however, dust becomes sublimated close to the star, within radius

$$R_i = 1.2\times 10^{15}\left(\frac{L}{L_{Sun}}\right)^{1/2} cm$$

- the luminosity of main sequence stars is

$$L \approx 10\left(M/M_{Sun}\right)^3 L_{Sun}, \qquad 7\,M_{Sun} < M < 20\,M_{Sun}$$

- there exists a zone where radiation pressure exceeds gravity provided that $M > 13\ M_{\mathrm{Sun}}$
- rotation alleviates the problem
  - higher ram pressure of disk accretion can overcom radiation pressure; radiation may also be beamed towards the poles thus reducing the pressure on the disk
- 3D simulations exhibit radiation driven Rayleigh-Taylor instability where radiation can escape through lower density regions

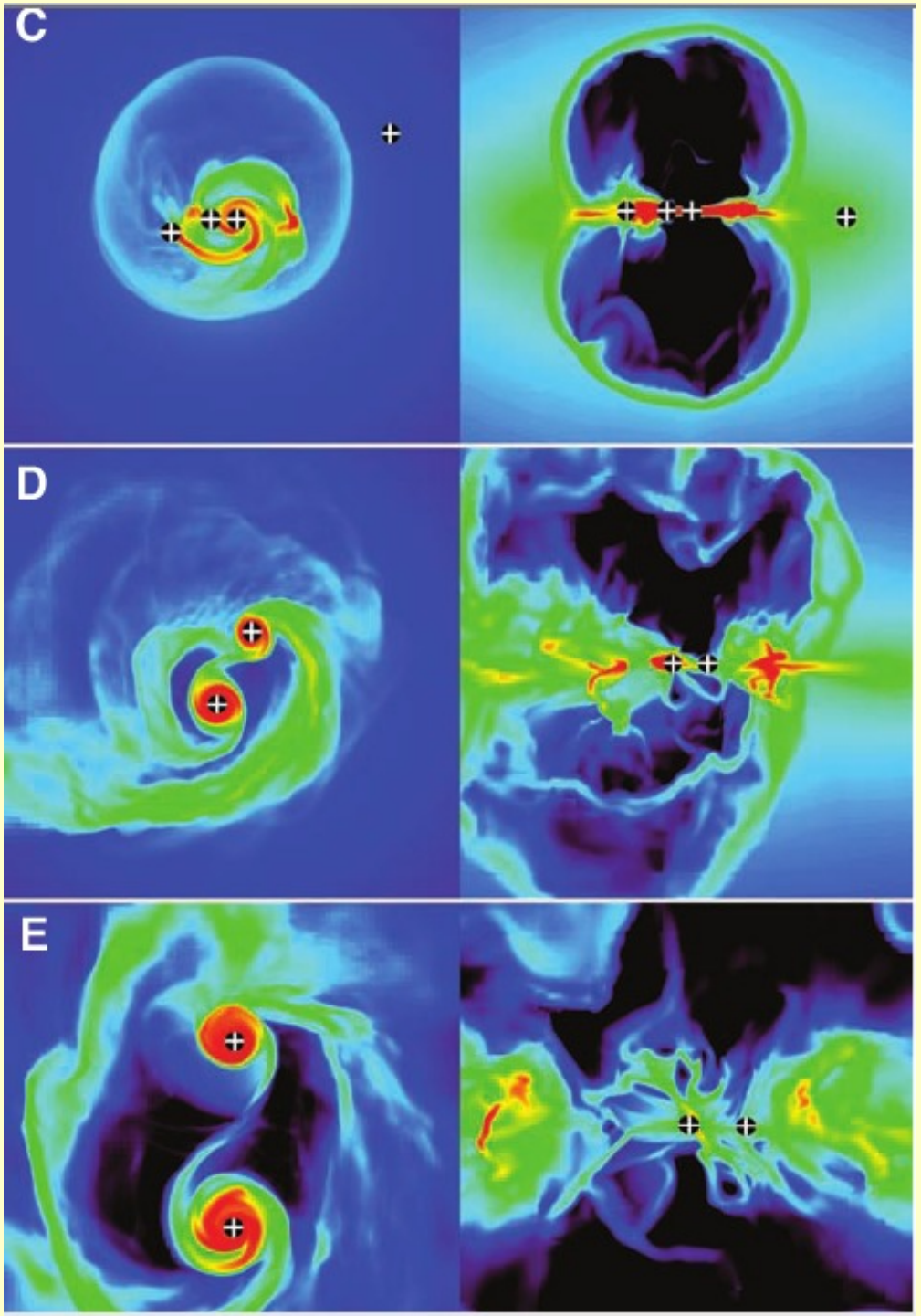

Krumholz (2009)

Krumholz (2009)

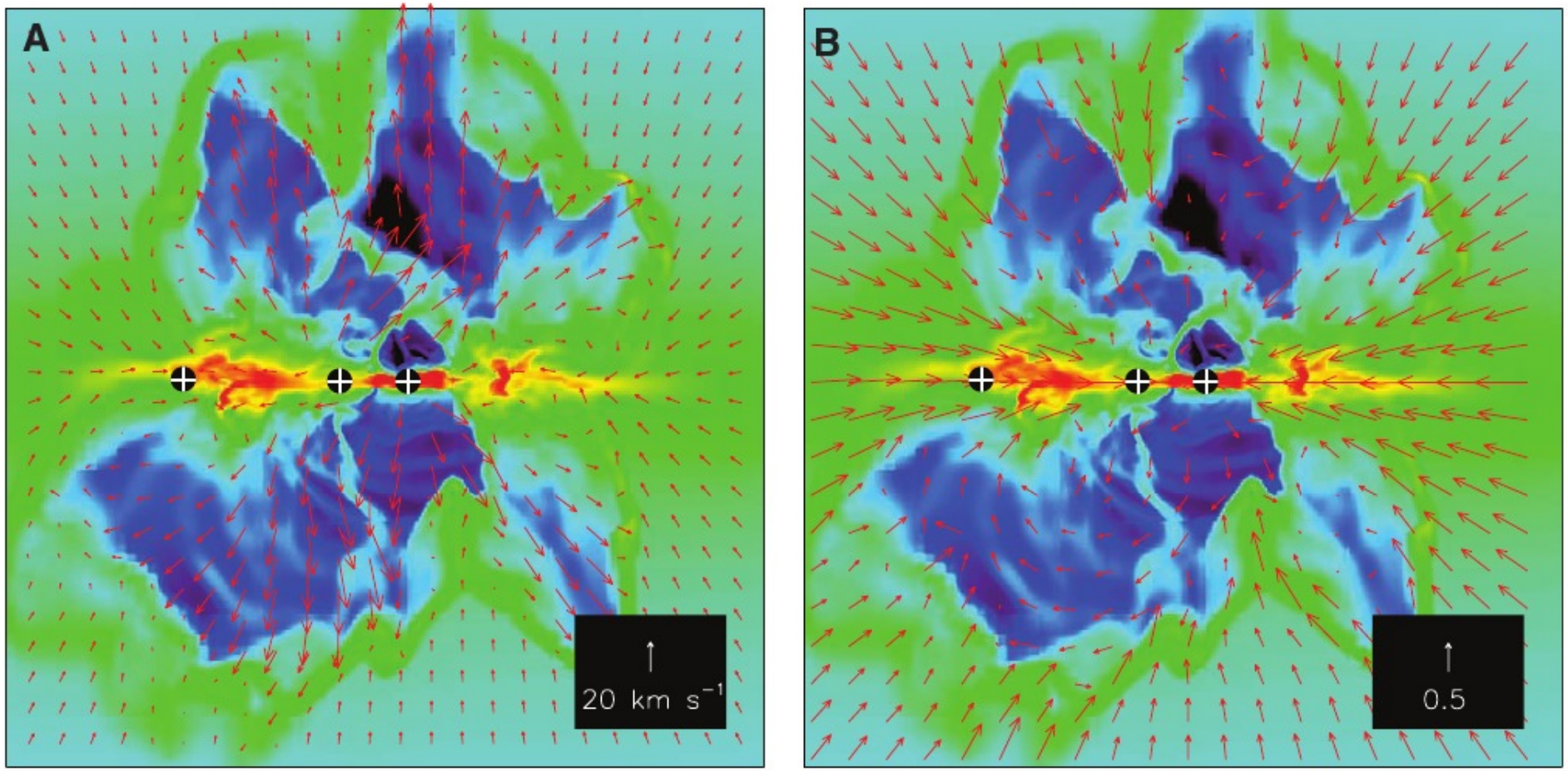

Fig. 3. Snapshot of a (6000 AU)^2 slice along the rotation axis at 51,100 years. Color indicates density from 10^{-20} to 10^{-14} g cm^{-3} on a logarithmic scale as in Fig. 1. Plus signs show projected stellar positions. (**A**) Arrows show gas velocity. (**B**) Arrow directions indicate the direction of the net (radiation plus gravitational) force; lengths are proportional to the magnitude of the net force divided by the magnitude of the gravitational force. Thus, an inward arrow of length 1 represents negligible radiation force.

Protostellar classes

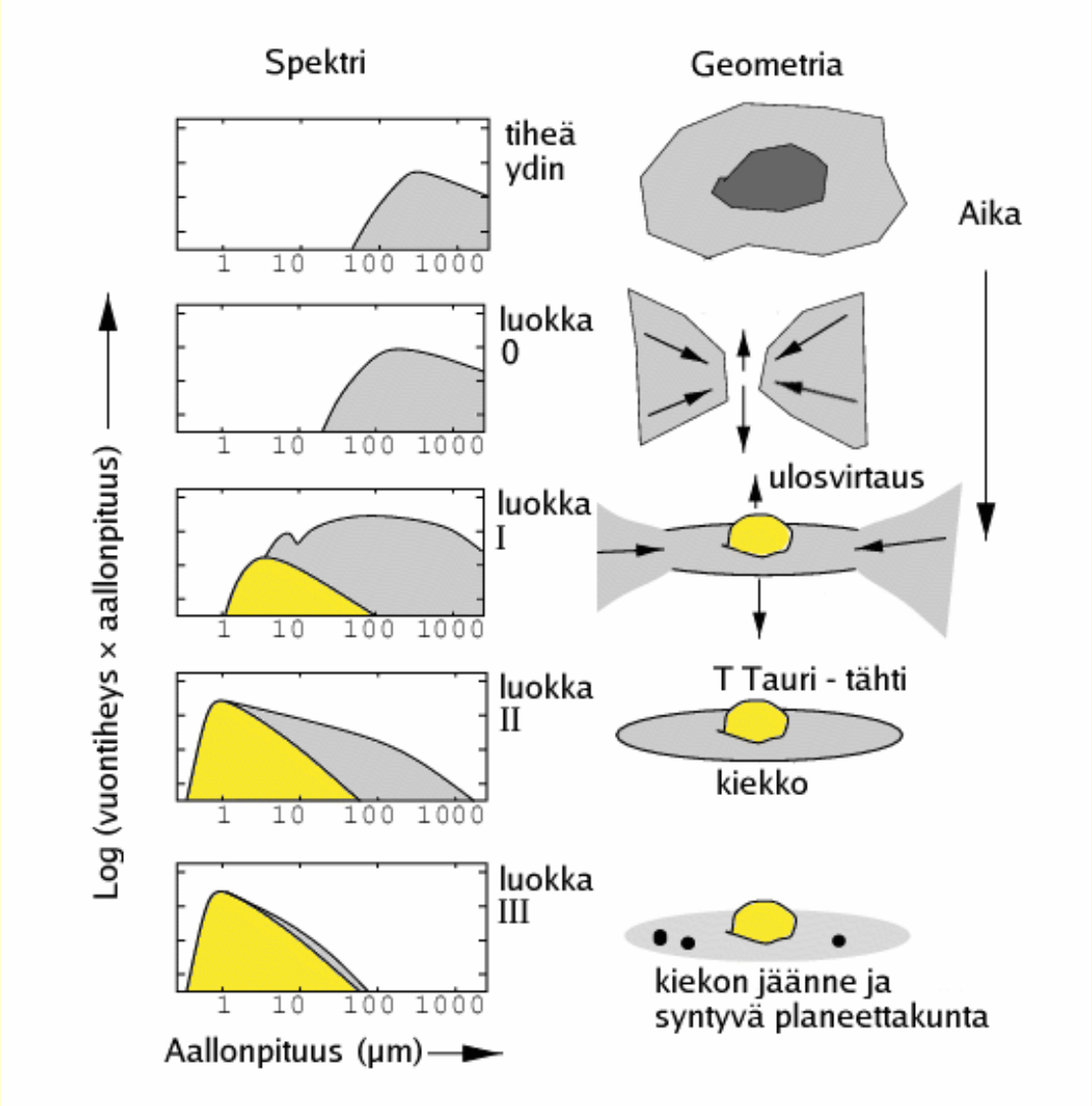

cores

protostars

pre-main sequence stars

main sequence stars

Picture: M. Hogerheijde

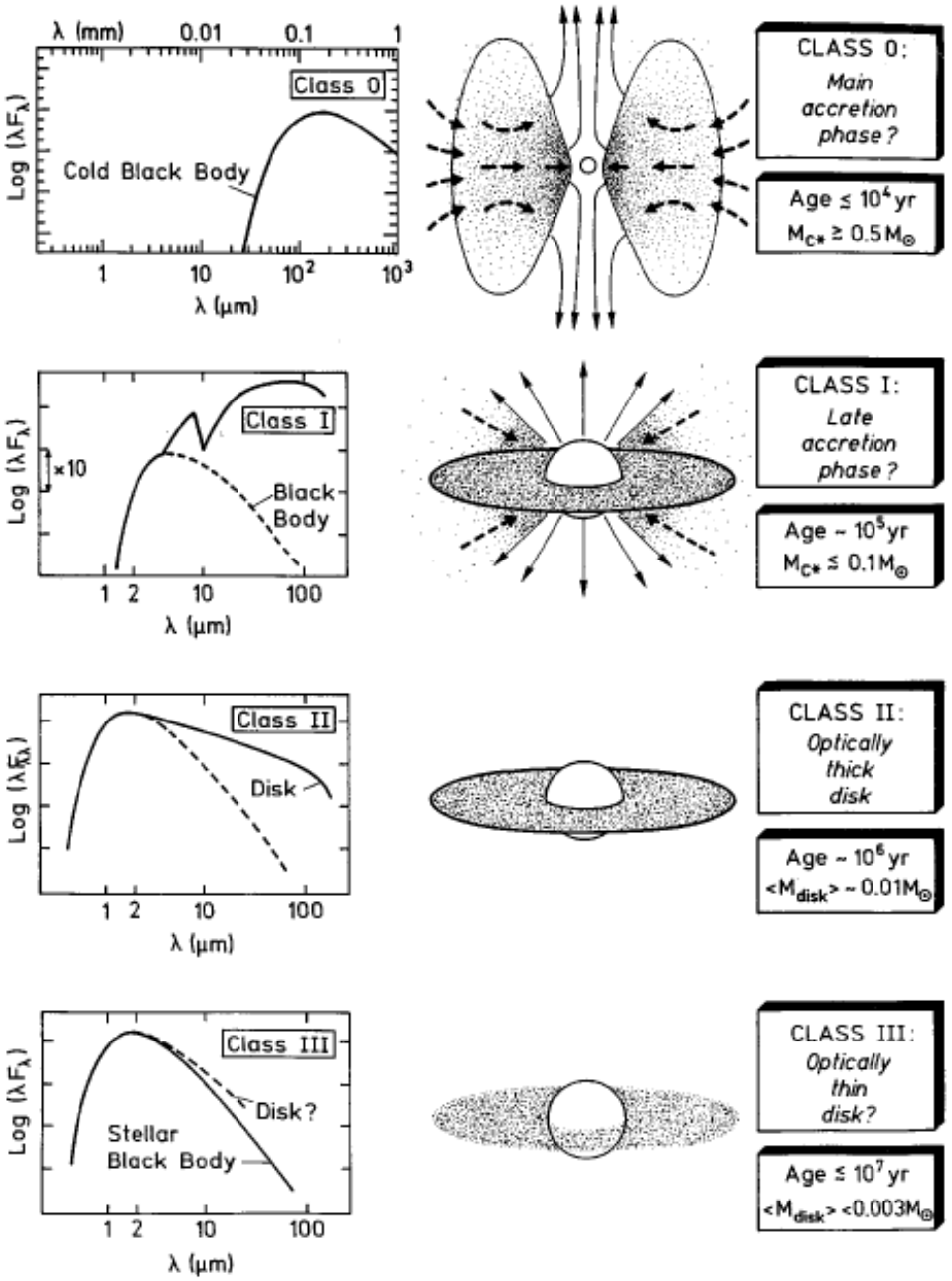

Figure 11 Evolutionary sequence of the spectral energy distributions for low-mass YSOs as proposed by André (1994). The four classes 0, I, II, and III correspond to successive stages of evolution.

Bachiller (1996)

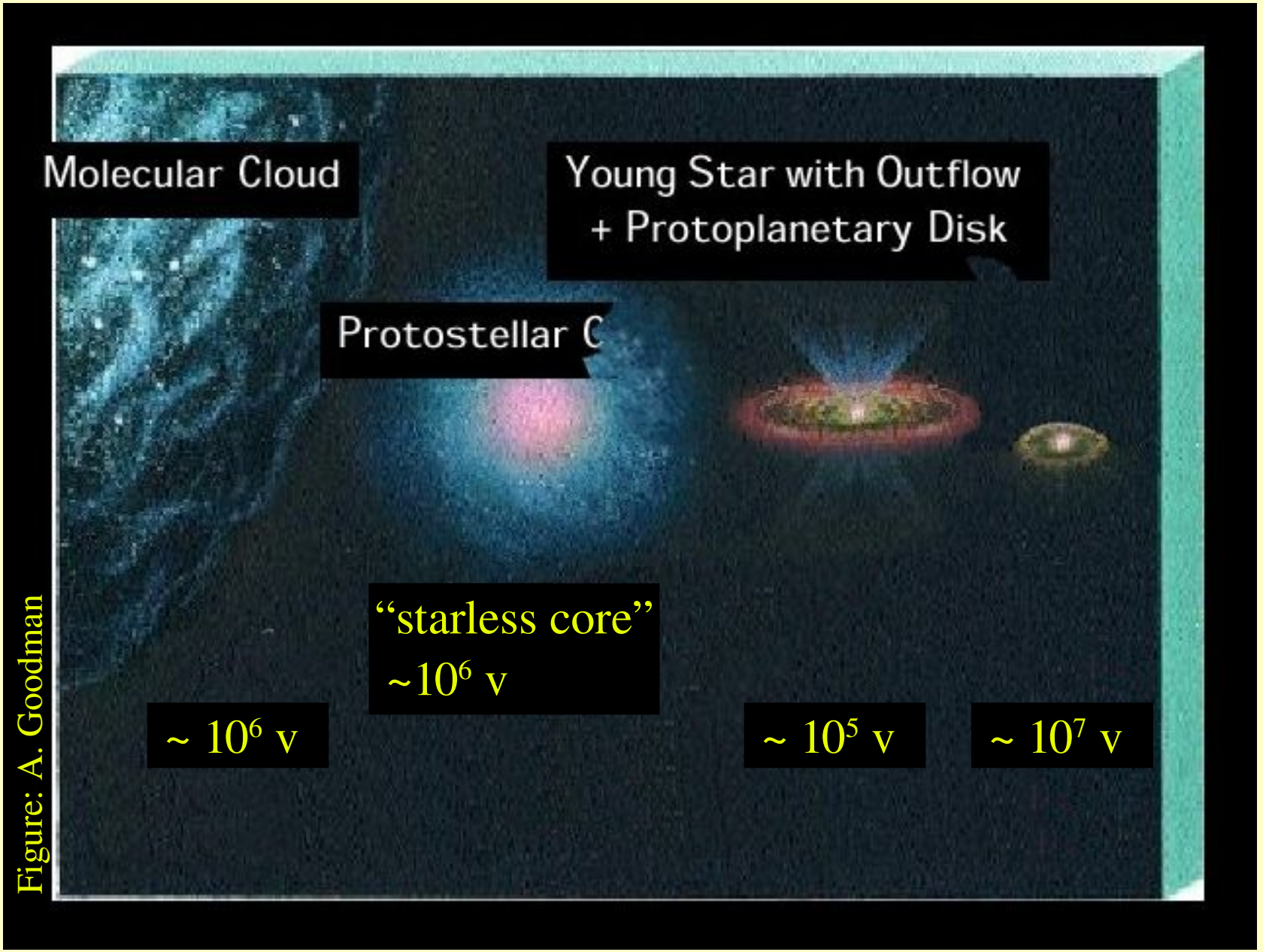

Figure: A. Goodman

Andre, Basu & Inutsuka 2008, astro-ph 0801-4210
The formation and evolution of prestellar cores
Bachiller 1996, ARAA 34, 111
Bipolar molecular outflows from young stars and protostars
Bate 2009, astro-ph 0811.0163
Combet et al. 2008, A&A 479, 481
Dullemond et al. 2007, astro-ph 0602619
Models of the structure and evolution of protoplanetary disks
Kratter et al. 2008, ApJ 681, 375
Krumholz et al., 2009, Science 323, 754
Larson 2003, Rep.Prog.Phys. 66, 1651
Lodato 2008, New Astron. Reviews 52, 21
Classical disc physics
Machida et al. 2007, ApJ 670, 1198
Matsumoto et al. 2004, ApJ 616, 266
McKee & Ostriker 2007, ARAA 45, 567
Theory of star formation
Shu 1977, ApJ 475, 251
Shu et al. 2003, Protostar & Planets IV, 789
Stahler, Palla: The formation of stars, Wiley-VCH (2004)
Ramos, Ceccarelli, Elitzur, 2007, A&A 471, 187

Excerpts from the latest Star Formation Newsletter...

The Star Formation Law in Atomic and Molecular Gas

Mark R. Krumholz[1], Christopher F. McKee[2] and Jason Tumlinson[3]

[1] Astronomy Department, University of California, Santa Cruz, CA 95064, USA
[2] Physics and Astronomy Departments, UC Berkeley, Berkeley, CA 94720 USA
[3] Space Telescope Science Institute, Baltimore, MD 21218 USA

E-mail contact: krumholz *at* ucolick.org

We propose a simple theoretical model for star formation in which the local star formation rate in a galaxy is determined by three factors. First, the interplay between the interstellar radiation field and molecular self-shielding determines what fraction of the gas is in molecular form and thus eligible to form stars. Second, internal feedback determines the properties of the molecular clouds that form, which are nearly independent of galaxy properties until the galactic ISM pressure becomes comparable to the internal GMC pressure. Above this limit, galactic ISM pressure determines molecular gas properties. Third, the turbulence driven by feedback processes in GMCs makes star formation slow, allowing a small fraction of the gas to be converted to stars per free-fall time within the molecular clouds. We combine analytic estimates for each of these steps to formulate a single star formation law, and show that the predicted correlation between star formation rate, metallicity, and surface densities of atomic, molecular, and total gas agree well with observations.

Accepted by ApJ

Protostar formation in supersonic flows: growth and collapse of spherical cores

Hao Gong & Eve C. Ostriker[1]

[1] Department of Astronomy, University of Maryland, College Park, MD, 20742-2421, USA

E-mail contact: hgong *at* astro.umd.edu, ostriker *at* astro.umd.edu

We present a unified model for molecular core formation and evolution, based on numerical simulations of converging, supersonic flows. Our model applies to star formation in GMCs dominated by large-scale turbulence, and contains four main stages: core building, core collapse, envelope infall, and late accretion. During the building stage, cores form out of dense, post-shock gas, and become increasingly centrally stratified as the mass grows over time. Even for highly-supersonic converging flows, the dense gas is subsonic, consistent with observations showing quiescent cores. When the shock radius defining the core boundary exceeds $R \approx 4a(4\pi G\rho_{mean})^{-1/2}$, where a is the isothermal sound speed, a wave of collapse propagates from the edge to the center. During the building and collapse stages, density profiles can be fit by Bonnor-Ebert profiles with temperature 1.2 - 2.9 times the true value, similar to many observed cores. As found previously for initially static equilibria, outside-in collapse leads to a Larson-Penston density profile $\rho \approx 8.86a^2/(4\pi Gr^2)$. The third stage, consisting of an inside-out wave of gravitational rarefaction leading to $\rho \propto r^{-3/2}$, $v \propto r^{-1/2}$, is also similar to that for initially-static spheres, as originally described by Shu. We find that the collapse and infall stages have comparable duration, $\sim t_{ff}$, consistent with estimates for observed prestellar and protostellar (Class 0/I) cores. Core building takes longer, but does not produce high-contrast objects until shortly before collapse. The time to reach core collapse, and the core mass at collapse, decrease with increasing inflow Mach number. For all cases the accretion rate is $\gg a^3/G$ early on but sharply drops off; the final system mass depends on the duration of late-stage accretion, set by large-scale conditions in a cloud.

Accepted by ApJ

http://arxiv.org/abs/0904.3568

What does a universal IMF imply about star formation?

Simon P. Goodwin[1] **and M.B.N. Kouwenhoven**[1]

[1] Department of Physics and Astronomy, University of Sheffield, Hicks Building, Hounsfield Road, Sheffield S3 7RH, UK

E-mail contact: s.goodwin *at* sheffield.ac.uk

We show that the same initial mass function (IMF) can result from very different modes of star formation from very similar underlying core and/or system mass functions. In particular, we show that the canonical IMF can be recovered from very similar system mass functions, but with very different mass ratio distributions within those systems. This is a consequence of the basically log-normal shapes of all of the distributions. We also show that the relationships between the shapes of the core, system, and stellar mass functions may not be trivial. Therefore, different star formation in different regions could still result in the same IMF.

Accepted by MNRAS

http://arxiv.org/abs/0904.4619